Nuclear structure of ^{82}Kr and ^{82}Se relevant for neutrinoless double-beta decay

Udo Gayer[1,*], *Volker* Werner[1,**], *Tobias* Beck[1], *Sean* Finch[2], *Jörn* Kleemann[1], *Krishichayan*[2], *Bastian* Löher[1], *Oliver* Papst[1], *Norbert* Pietralla[1], *Philipp Christian* Ries[1], *Deniz* Savran[3], *Michael* Weinert[4], and *Werner* Tornow[2]

[1]Institut für Kernphysik, Technische Universität Darmstadt, Darmstadt, HE, Germany
[2]Department of Physics, Duke University and Triangle Universities Nuclear Laboratory, Durham, NC, USA
[3]GSI Helmholtzzentrum für Schwerionenforschung, Darmstadt, HE, Germany
[4]Institut für Kernphysik, Universität zu Köln, Köln, NRW, Germany

Abstract. Nuclear Resonance Fluorescence (NRF) experiments on the nuclei ^{82}Kr and ^{82}Se were performed, that are a candidates for a mother-daughter pair for the hypothetical neutrinoless double-beta ($0\nu\beta\beta$) decay. The experiment aimed at providing high-precision data to benchmark theoretical calculations of the nuclear matrix elements involved in this exotic decay mode. We have investigated the excitation energy range from 2.3 MeV to 4.2 MeV, where the nuclear scissors mode is expected to be located in nuclei of this mass region. Our experiment was able to constrain decay branches of the scissors mode down to a level of a few percents, comparable to previous experiments on heavy deformed $0\nu\beta\beta$ decay candidates. Reduced transition strengths of the magnetic dipole-excited states have been determined by a method that exploits the non-resonant background in the NRF spectra. They are compared to a calculation within the nuclear shell model for ^{82}Se, which reveals their mixed orbital and spin character, hinting at a more complex microscopic structure of low-lying 1^+ states.

1 Introduction

Neutrinoless double-beta ($0\nu\beta\beta$) decay is a hypothesized second-order weak interaction process [1] which could occur if the neutrino is its own antiparticle, a so-called Majorana particle [2]. Furthermore, the decay rate $\lambda_{0\nu\beta\beta}$ for $0\nu\beta\beta$ decay is approximately proportional to the square of the effective Majorana mass $\langle m_{\beta\beta}\rangle$ of the electron neutrino [3]:

$$\lambda_{0\nu\beta\beta} = G_{0\nu}(Q_{\beta\beta}, Z)|M_{0\nu}|^2\langle m_{\beta\beta}\rangle^2 \quad (1)$$

The proportionality constants in Eq. (1) are a known phase space factor $G_{0\nu}$ which depends on the decay Q-value and the electric charge Z of the mother nucleus, and the nuclear matrix element $M_{0\nu}$ involved in the decay.

A potential candidate for non-standard model physics and direct probe of the neutrino mass, the observation of $0\nu\beta\beta$ decay is the aim of a multitude of experimental collaborations. Recently, new results have been published for a variety of isotopes by different collaborations, for example CUPID-0 [4], EXO-200 [5], GERDA [6] and NEMO3/SuperNEMO [7, 8], reporting lower limits for $0\nu\beta\beta$ half-lives up to the order of 10^{26} y. For the pair of nuclei under investigation in this experiment, the CUPID-0 experiment [4] improved the previous lower limit of the NEMO3 collaboration [9] by more than one order of magnitude from 1.0×10^{23} y to 2.4×10^{24} y, confirming ^{82}Se as one of the most promising detector materials.

However, estimations of decay rates for a certain nucleus and, ultimately, the precision of an extracted neutrino mass, depend on the most uncertain quantity on the right-hand side of Eq. (1): the nuclear matrix element $M_{0\nu}$. Since this matrix element could only be measured directly in $0\nu\beta\beta$ decay if the neutrino mass was known, it has to be provided by nuclear theory at the moment. Reference [10] gives an overview of the current efforts to calculate $M_{0\nu}$ using different theoretical models. In their evaluation, Engel and Menéndez find that the overall agreement of the models is within a factor 2-3. But there are clearly systematic deviations between them. Comparing just the differences between theories, predicted decay rates can vary by up to an order of magnitude, which requires a huge experimental effort to cope with. Therefore, more accurate estimates of nuclear matrix elements are desirable, which, in turn, need precise nuclear data as benchmarks.

Nuclear structure experiments that aim to improve the data on $0\nu\beta\beta$ candidates follow two different approaches: The first is to measure analog reactions like double charge-exchange reactions [11] that use a similar model space in reaction calculations as $0\nu\beta\beta$ decay. Though very close to the actual nuclear process, experiments of this kind are challenging to perform and the interpretation of the data is not model-independent. In this experiment we follow the second approach to use a well-established reaction mechanism to study the structure of nuclei involved in $0\nu\beta\beta$ decay with high precision. We chose the method of Nuclear Resonance Fluorescence (NRF), an electromagnetic process which is well-understood and from whose observables nuclear properties can be extracted quasi model-independently [12].

*e-mail: ugayer@ikp.tu-darmstadt.de
**e-mail: vw@ikp.tu-darmstadt.de

Previous studies [13, 14] have shown that shape coexistence and shape mixing in nuclei have a large influence on $M_{0\beta}$ and may even lead to significant branching of the $0\nu\beta\beta$ decay to excited states in the daughter nucleus. An experimental observable which is sensitive to shape coexistence effects is the decay of mixed-symmetric magnetic dipole excitations, called the scissors mode [15, 16] in deformed nuclei. Figure 1 shows a schematic calculation in the Interacting Boson Model 2 (IBM-2) [17], which is a well-established model for studies of the scissors mode and the phenomenology of the evolution of nuclear structure with nucleon numbers. In Fig. 1, the control parameter for the phase transition between a spherical vibrator and a rigid rotor has been varied for a ^{82}Se-like nucleus. The quantity of interest is the ratio of the partial transition widths Γ_i to the ground state and the first excited 0^+ state. It is obvious that the branching depends strongly on the nuclear shape, indicating that this is indeed a useful observable to study the evolution of shapes in nuclei. Because the scissors mode, as a collective excitation, manifests itself in few, well separated, strongly dipole-excited states not too far away from shell closures, NRF is an ideal tool to investigate its decay behavior.

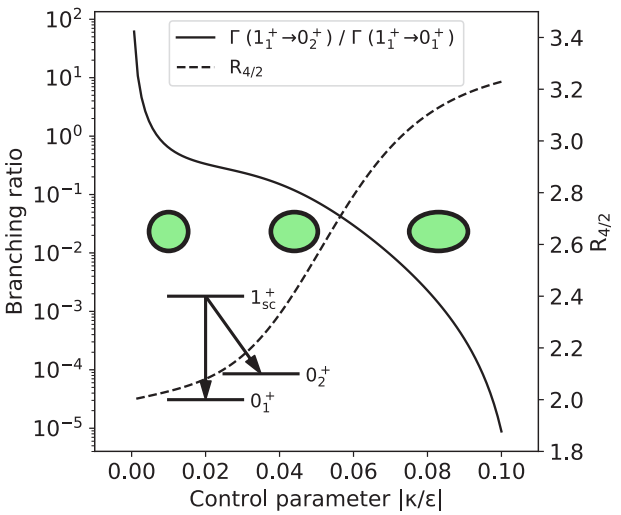

Figure 1. Schematic evolution of the intensities of the scissors mode decay branches to the ground state and the first excited 0^+ state for a ^{82}Se - like nucleus, using the IBM-2 Hamiltonian from [14] with $c_\pi^{(L)} = 0$. The ratio on the x-axis is a control parameter in the IBM for the shape phase transition from a spherical vibrator to a rigid rotor (indicated as an ellipse with increasing asymmetry in the figure). The Majorana parameters were fixed to set the energy of the 1^+_{sc} state at about 3.5 MeV (varying κ/ϵ does not influence this value too much), χ was set to $-\sqrt{7}/2$. Simultaneously with the branching ratio, the $R_{4/2}$ ratio, another indicator for the nuclear shape, is shown as a dashed line.

Before the experiment described in this contribution, no comprehensive study of the dipole response of the ^{82}Kr and ^{82}Se had been performed. Information about low-lying dipole-excitations in both nuclei was restricted to two $J = 1$ excitations in ^{82}Se from a bremsstrahlung NRF experiment at the Stuttgart Dynamitron [18] with an endpoint energy of about 3.1 MeV [19].

This contribution is divided into a description of the experimental setup and the analysis procedure, followed by a discussion of the preliminary data and a conclusion.

2 Experiment

The experiment was performed in fall 2016 at the High-Intensity γ-Ray Source (HIγS) [20] at the Triangle Universities Nuclear Laboratory (TUNL). Using the small-bandwidth, almost 100 % linearly polarized photon beam of HIγS, polarimetry of isolated dipole-excited states becomes straightforward [21]. With a dedicated experimental setup [22], precise studies of their decay properties are possible [23].

Because the probability of the beam reacting with a single NRF target was sufficiently low, it was possible to use a second, parasitic setup and measure the dipole response of both nuclei at the same time. The upstream target consisted of 1.99845(7) g of selenium, enriched to 99.93 % in ^{82}Se. As a powder in the chemical compound SeO_2, it was filled in a target container made of polyvinylchloride (PVC). It was mounted in the γ^3 setup [22], employing four High-purity Germanium (HPGe) detectors at observation angles of ($\theta = 90°$, $\varphi = 0°$), (90°, 90°), (135°, 45°), and (135°, 135°). Here, the angle θ is the polar angle w.r.t the beam axis and φ the corresponding azimuthal angle. The downstream target was a stainless steel sphere with an outer radius of 2 cm filled with 1.50218(11) g of pure krypton gas enriched to 99.945 % in ^{82}Kr. Because the target container had a comparably high mass of about 10 g, an identical empty sphere was used to corroborate the origin of gamma-rays from ^{82}Kr. The second target was mounted in a setup with four HPGe detectors at angles of ($\theta = 90°$, $\varphi = 0°$), (90°, 90°), (90°, 180°) and (90°, 270°).

Anticipating the energy range of the scissors mode in ^{82}Kr and ^{82}Se from previous experiments [19] and systematics [24] (which have been shown to hold also for medium-mass nuclei [25]), we have scanned the energy range from 2.40(8) MeV to 4.10(15) MeV (the uncertainties indicate the FWHM of the HIγS beam which increased continuously with energy).

At each energy setting, both targets were irradiated for about 3-4 h. Having identified strongly excited 1^+ states in ^{82}Kr and ^{82}Se, we further irradiated for about 29 h at 2.98(10) MeV and about 16 h at 3.82(13) MeV to get precise information about their decay behaviors.

3 Analysis

Figure 2 shows the accumulated statistics of selected detectors in both setups at a beam energy of 3.82(13) MeV. Conveniently, at this energy, excited 1^+ states have been observed both in ^{82}Kr and ^{82}Se. The number of counts A_n in each detector n at a photon energy $E_\gamma = E_k - E_f$ is given by:

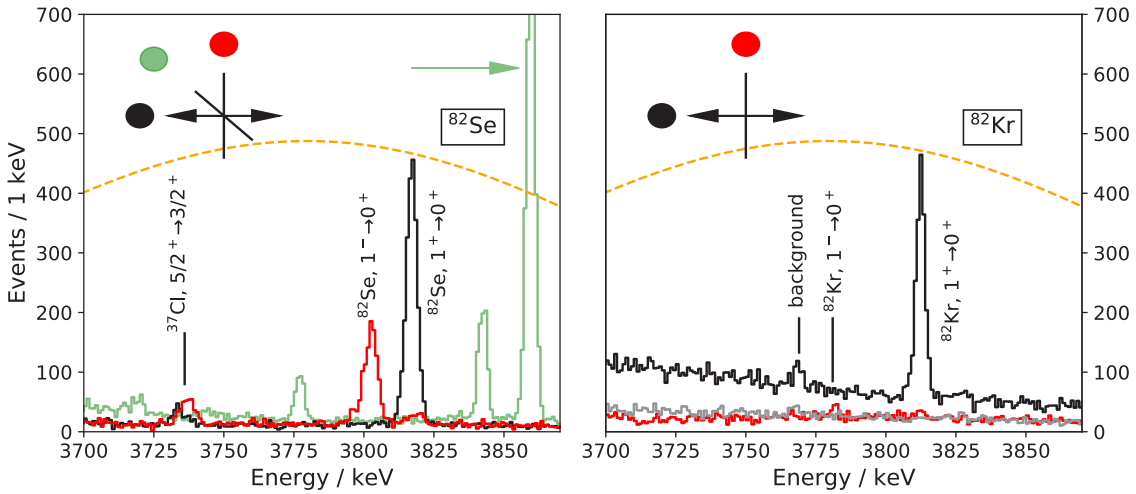

Figure 2. NRF spectra from photon scattering off the ^{82}Se (left) and ^{82}Kr targets (right) at a beam energy of 3.82(13) MeV in detectors at different angles (the green spectrum of the backward angle detector has been shifted by 40 keV for better visibility). The detector position with respect to the polarization axis (double arrow) is indicated by the color code in the inset drawing. A diagonal line in the inset means the detector was at a backward angle of $\theta = 135°$. The beam intensity distribution is indicated by a dashed orange line. The strong sensitivity of the angular distribution to the parity of dipole-excited states can be seen by comparing the count rate of the detectors mounted in the polarization plane of the beam (black) and perpendicular to it (red). Along with the spectra of the ^{82}Kr experiment, a summed spectrum of a measurement with an empty gas sphere is shown in grey, which identifies the line at 3769 keV as a contamination from the container.

$$A_n(E_k - E_f) = N_T \cdot N_\gamma(E_k) \cdot \epsilon_n(E_k - E_f) \cdot \qquad (2)$$

$$I_{0^+ \to J_k^{\pi_k} \to J_f^{\pi_f}} \cdot \tilde{w}(\theta_n, \varphi_n, \{J, \pi, \delta\})$$

In Eq. (2), an excitation from a 0^+ ground state to a state $J_k^{\pi_k}$ with subsequent deexcitation to a state $J_f^{\pi_f}$ is assumed. The symbol N_T denotes the number of target nuclei hit by the beam, $N_\gamma(E_k)$ is the beam intensity at the excitation energy, $\epsilon(E_\gamma)$ is the detection efficiency at the energy of the emitted photon, I is the integrated cross section of this sequence of transitions, and $\tilde{w}$ its angular distribution, which depends on the involved quantum numbers of the levels, the multipole mixing ratio δ of the transition $k \to f$, and the geometry of the setup.

Both the assignments of angular momentum- and parity quantum numbers to unknown states and the determination of multipole mixing ratios were achieved by the analysis of angular correlations. For this, the experimental asymmetry ϵ_{mn} of the count rates A_m and A_n,

$$\epsilon_{mn} = \frac{A_m - A_n}{A_m + A_n} = \qquad (3)$$

$$\frac{\epsilon_m(E_\gamma) \cdot \tilde{w}(\theta_m, \varphi_m, \{J, \pi, \delta\}) - \epsilon_n(E_\gamma) \cdot \tilde{w}(\theta_n, \varphi_n, \{J, \pi, \delta\})}{\epsilon_m(E_\gamma) \cdot \tilde{w}(\theta_m, \varphi_m, \{J, \pi, \delta\}) + \epsilon_n(E_\gamma) \cdot \tilde{w}(\theta_n, \varphi_n, \{J, \pi, \delta\})}$$

is determined for all detector pairs $\{m, n\}$, and compared to theoretical values ϵ_{theo}. In the second part of Eq. (3), A has been replaced using Eq. (2), leaving only the geometry-dependent factors. The values of ϵ_{theo} were obtained by implementing all important parts of the HIγS upstream target room and all angular distributions [26] in the Geant4 [27–29] framework.

The simulations for ϵ alone were validated by comparison to measurements with radioactive ^{56}Co and ^{152}Eu sources. It was found that the energy dependence of the detection efficiency was reproduced well for each detector. The ratio of efficiencies ϵ_m/ϵ_n of detector pairs was reproduced by the numerical simulations up to a constant factor of < 1.5, which may be caused by deficient charge collection in the detectors and the signal processing electronics, both of which are not simulated by Geant4. We used the measured ratio of efficiencies to correct for this.

The simulations for the product $\epsilon \cdot \tilde{w}$ were validated by comparison of ϵ_{theo} to known values of J, π and δ for transitions of ^{82}Se [19], ^{35,37}Cl [30, 31] and ^{56}Fe [32] (the latter were constituents of the PVC target container and the stainless steel gas container). All values known from literature were reproduced within the statistical uncertainties. Figure 3 shows the determination of the quantum numbers J and π for the newly observed 1_4^+ state of ^{82}Se by the asymmetry of its ground-state transition.

With the knowledge of the spin and parity quantum number and the multipole mixing ratio of a transition, Eq. (2) also allows for the determination of excitation cross sections, if the beam intensity distribution N_γ is known. Unfortunately, a direct measurement of the beam intensity with an unattenuated zero-degree detector is not possible due to the high overall intensity. Furthermore, a normalization to a known cross section could only be done for one energy setting in the ^{82}Se experiment, where the transition from Ref. [19] was observed, and for none in the ^{82}Kr experiment.

In this work, we chose to estimate the absolute beam intensity by analyzing the non-resonant background in the spectra. This background is mostly caused by beam photons scattering off the targets and the residual air in the

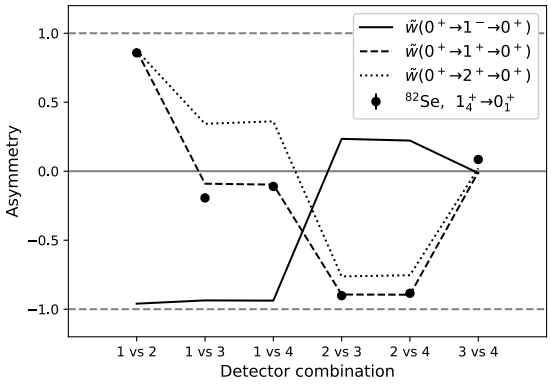

Figure 3. Asymmetry of the ground state transition of a ^{82}Se state at 3822 keV between all possible detector pairs (labeled with numbers 1-4, corresponding to the order in which they appear in the text). The theoretical minimum and maximum possible asymmetries -1 and 1 are indicated by horizontal dashed lines. The solid, dashed, and dotted lines show the simulated asymmetries assuming different angular momentum and parity quantum numbers of the excited state.

evacuated beam pipe into the detectors and it is responsible for more than 99 % of the count rate. We have modeled the beam-induced background in a virtual experiment using Geant4 by impinging a beam with a realistic intensity distribution onto the setup, assuming that the non-resonant scattering cross section σ_{nonres} is composed of the cross sections for the photoeffect (σ_{ph}), e^+/e^- pair production (σ_{pp}), Compton scattering (σ_{c}), and Rayleigh scattering (σ_r):

$$\sigma_{\text{nonres}} \approx \sigma_{\text{ph}} + \sigma_{\text{pp}} + \sigma_{\text{c}} + \sigma_{\text{r}} \tag{4}$$

This simulation yields energy spectra $A^{(1)}_{\text{nonres,sim}}(E)$ for each detector. The notation $A^{(1)}$ indicates that Geant4 is able to resolve every single event, which is not true in reality. To account for these pile-up effects, we interpreted $A^{(1)}_{\text{nonres,sim}}(E)$ as a probability distribution and calculated the convolution with itself to get the distribution for higher-multiplicity events:

$$A^{(k)}_{\text{nonres,sim}}(E) = \left(A^{(k-1)}_{\text{nonres,sim}} * A^{(1)}_{\text{nonres,sim}}\right)(E) \tag{5}$$

As shown in Fig. 4 the contribution of events with $k \geq 3$ was always negligible in accordance with the measured dead times of less than 20 % during the experiment, therefore only $k \in \{1, 2, 3\}$ was used in this analysis. Further contributions which are not directly caused by the beam are background caused by the detector response to the real NRF events A_{NRF} and from natural radioactivity and cosmic radiation A_{bg}. The effect of A_{NRF} was taken into account by simulating a target radiating photons with the corresponding energies and angular distributions of all observed NRF lines.

The natural and cosmic background was determined by off-beam measurements and normalized to the in-beam measurement via the ratio of live times $a_0 = t_{\text{live,beam}}/t_{\text{live,no beam}}$. In total, a sum of 4 background contributions was fit to the experimental spectra using the fit parameters a_1 to a_4:

$$A_{\text{nonres,sim}} = \underbrace{\frac{t_{\text{live,beam}}}{t_{\text{live,no beam}}}}_{a_0} \cdot A_{\text{bg}} + a_1 \cdot A^{(1)}_{\text{nonres,sim}} \tag{6}$$

$$+a_2 \cdot A^{(2)}_{\text{nonres,sim}} + a_3 \cdot A^{(3)}_{\text{nonres,sim}} + a_4 \cdot A_{\text{NRF}}$$

The fit was weighted with the statistical uncertainty of the bin contents in the experimental spectrum. Since the background increases almost exponentially towards lower energies, this region dominates the result. Nevertheless, the high-energy, non-resonant background depends weakly on the density $\rho_{\text{air,res}}$ of the residual air in the beam pipe, because this causes small-angle Compton scattering of beam photons into the detectors. By comparing to the high-energy background, we found that $\rho_{\text{air,res}}$ was about two orders of magnitude lower than the density of air at standard conditions. An example for a fit can be seen in Fig. 4.

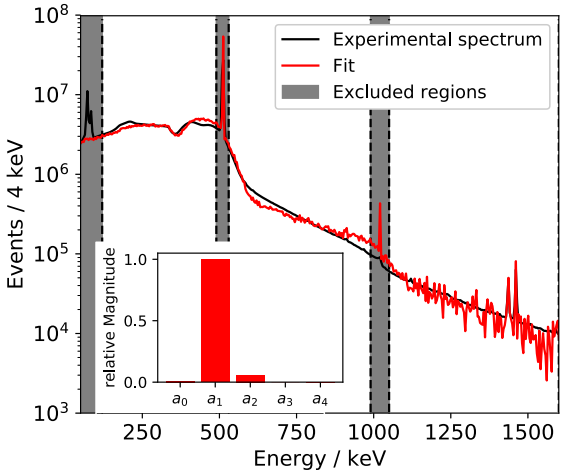

Figure 4. Fit of the experimental spectrum of the HPGe detector at $\theta = 90°$ and $\varphi = 0°$ with a simulated background spectrum as described in the text. The grey bars show regions which were excluded from the fit. The single- and double-escape lines at 511 keV and 1022 keV were excluded, because they would dominate the fit and make the overall visual agreement worse. Furthermore, the x-ray resonances at about 100 keV and everything below were excluded, because this effect was not included in the simulation. The inset shows the relative magnitude of the fit parameters a_i, assuming the corresponding background contribution is normalized ($\int A dE = 1$).

With known parameters a_i, the number of incident beam photons can be calculated in a straightforward way, using the intensity distribution of simulated primary particles $N_0(E_k)$, which is directly proportional to the statistics in the simulated spectrum:

$$N_\gamma(E_k) = N_0(E_k) \sum_{i \in \{1,2,3\}} a_i \tag{7}$$

Between the four detectors in each setup at a single beam energy setting, the reconstructed beam intensities all agree

within a factor of 2 from their weighted mean value, which is our conservative estimate of the systematic uncertainty of this procedure. Using N_γ from this analysis, it is possible to determine absolute cross sections for all observed transitions. Only the ground-state cross section $I_{0^+\to1^+\to0^+}$ for a state of ^{82}Se at a beam energy of 2.98 MeV could be determined both in this work and in Ref. [19]. Within the large systematic uncertainty that was determined here, both results agree. Nevertheless, it would be desirable to have a dedicated measurement, probably with bremsstrahlung NRF, for the elastic cross sections in ^{82}Kr and ^{82}Se. Despite the large uncertainty, the method to determine the beam intensity described here has the advantage that it can be used without any additional detection systems or reference samples.

Branching ratios $\Gamma_{k\to f}/\Gamma_{k\to0}$ could be determined if a branching transition to a low-lying excited state f was observed in the spectra. Using the relation of I and the partial transition widths (see, e.g. [12]), the branching ratios can be obtained from a ratio of count rates using Eq. (2):

$$\frac{\Gamma_f}{\Gamma_0} = \frac{A_n(E_k - E_f)}{A_n(E_k)} \cdot \frac{\epsilon_n(E_k)\cdot\tilde{w}(\theta_n,\varphi_n, 0\to k\to 0)}{\epsilon_n(E_k - E_f)\cdot\tilde{w}(\theta_n,\varphi_n, 0\to k\to f)} \tag{8}$$

Equation (8) is independent of the beam intensity, i.e. the precision is only limited by counting statistics. Even at the two beam energy settings of 2.98(10) MeV and 3.82(13) MeV, where strongly excited 1^+ states were observed in both isotopes, no statistically significant transition to an excited 0^+ state was found. In such cases, an upper limit can be determined from the applied confidence level which demands that, after the subtraction of the smooth experimental background, a potential transition in a spectrum should contain more than $2\sigma_{\mathrm{bg}}$ events, where σ_{bg} denotes the statistical uncertainty of the subtracted background below the transition of interest. Using this criterion, we can constrain the branching of 1^+ states in both isotopes to be smaller than 5 % at the two beam energies mentioned above. However, we found branching transitions of excited 1^+ states to low-lying 2^+_1 and 2^+_2 states. In ^{82}Se, the decay branching ratios Γ_i/Γ_0 differ strongly by more than a factor of two for different 1^+ states.

4 Discussion

The findings in the last section about the energy dependence of the branching of 1^+ states and the total absence of branchings to the 0^+_2 states in both isotopes hint at a more complicated microscopic structure. First of all, the missing branchings are in disagreement with the simple IBM-2 picture from Sec. 1, because ^{82}Kr and ^{82}Se are not well-deformed nuclei. Secondly, the decay behavior of the 1^+ states of ^{82}Se would not be expected to show a strong energy dependence, if they were fragments of the same collective excitation.

Recently, the nuclear shell model was used successfully to interpret the structure of a 1^+ state in the medium-heavy nucleus ^{50}Cr [25]. Motivated by this, we have performed two calculations for ^{82}Se using the code

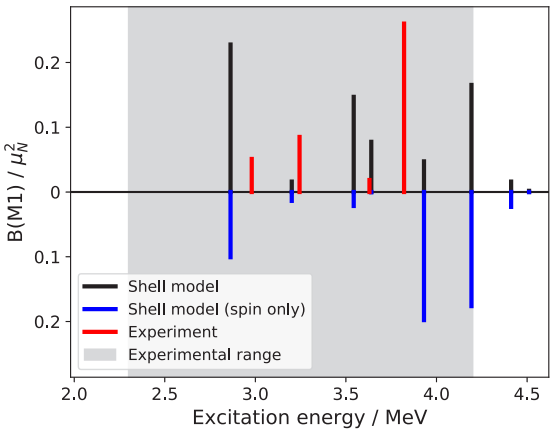

Figure 5. Experimental values for the $B(M1)\uparrow$ strengths of 1^+ states from the ground state in ^{82}Se, compared to a shell model calculation described in the text. The grey area indicates the energy range which was accessible in the experiment. On the mirrored y-axis, $B(M1)\uparrow$ has been calculated for the shell model states using only the spin part of the M1 operator.

NuShellX@MSU [33] with the jun45 interaction [34] in the complete so-called jj44 model space. In the first calculation, all g-factors which appear in the magnetic dipole operator were set to their bare values. In the second, the orbital g-factor of the proton was set to zero to be able to see only the contribution of the spin-part of the M1 operator, which causes spin-flip transitions between the $p_{3/2}$ and $p_{1/2}$ orbits in this model space.

The resulting reduced transition strengths $B(M1)\uparrow$ are shown in Fig. 5 in comparison to preliminary experimental values. Concerning the summed strength in this energy range and the onset of the 1^+ states of ^{82}Se, the calculation is in good agreement with the experiment. It implies a strong admixture of spin strength, even at lower energies, which varies strongly from state to state. This first analysis could explain the non-uniformity of the decay behaviour of the 1^+ states and also the preference for decays back to the ground state.

5 Conclusion

In conclusion, the decay branching ratios of low-lying dipole-excited state in ^{82}Se and ^{82}Kr have been determined with a precision on a level of a few percent. Excitation cross sections could be estimated for all states using a method that does not need additional calibration targets or detectors. Concerning the motivation to constrain theoretical models for the prediction of $0\nu\beta\beta$ decay matrix elements, the current state of our data suggests a more complicated structure of magnetic dipole transition than expected by estimations in the IBM-2. This was corroborated by a preliminary shell model calculation.

The authors would like to thank R. Schwengner for help with the preparation of the krypton target and the accelerator crew of HIγS for providing excellent experimental conditions. This

work was supported by the Deutsche Forschungsgemeinschaft under research grant SFB 1245. UG acknowledges support by the Helmholtz Graduate School for Hadron and Ion Research of the Helmholtz Association.

References

[1] W.H. Furry, Phys. Rev. **56**, 1184 (1939)
[2] E. Majorana, Nuovo Cim. **14**, 171 (1937)
[3] F.T. Avignone, S.R. Elliott, J. Engel, Rev. Mod. Phys. **80**, 481 (2008)
[4] O. Azzolini, M.T. Barrera, J.W. Beeman, F. Bellini, M. Beretta, M. Biassoni, C. Brofferio, C. Bucci, L. Canonica, S. Capelli *et al.*, Phys. Rev. Lett. **120**, 232502 (2018)
[5] J.B. Albert, D.J. Auty, P.S. Barbeau, E. Beauchamp, D. Beck, V. Belov, C. Benitez-Medina, J. Bonatt, M. Breidenbach, T. Brunner *et al.* (The EXO-200 Collaboration), Nature **510**, 229 EP (2014)
[6] M. Agostini, A.M. Bakalyarov, M. Balata, I. Barabanov, L. Baudis, C. Bauer, E. Bellotti, S. Belogurov, A. Bettini, L. Bezrukov *et al.* (The GERDA Collaboration), Phys. Rev. Lett. **120**, 132503 (2018)
[7] R. Arnold, C. Augier, J.D. Baker, A.S. Barabash, A. Basharina-Freshville, S. Blondel, S. Blot, M. Bongrand, D. Boursette, V. Brudanin *et al.* (The NEMO-3 Collaboration), Phys. Rev. D **95**, 012007 (2017)
[8] R. Arnold, C. Augier, J. Baker, A.S. Barabash, A. Basharina-Freshville, M. Bong. and, V. Brudanin, A.J. Caffrey, S. Cebrián, A. Chapon *et al.*, Eur. Phys. J. C **70**, 927 (2010)
[9] R. Arnold, C. Augier, J. Baker, A. Barabash, G. Broudin, V. Brudanin, A.J. Caffrey, E. Caurier, V. Egorov, K. Errahmane *et al.*, Phys. Rev. Lett. **95**, 182302 (2005)
[10] J. Engel, J. Menéndez, Rep. Prog. Phys. **80**, 046301 (2017)
[11] F. Cappuzzello, C. Agodi, M. Cavallaro, D. Carbone, S. Tudisco, D. Lo Presti, J.R.B. Oliveira, P. Finocchiaro, M. Colonna, D. Rifuggiato *et al.*, Eur. Phys. J. A **54**, 72 (2018)
[12] U. Kneissl, H. Pitz, A. Zilges, Prog. Part. Nucl. Phys. **37**, 349 (1996)
[13] T.R. Rodríguez, G. Martínez-Pinedo, Phys. Rev. Lett. **105**, 252503 (2010)
[14] J. Beller, N. Pietralla, J. Barea, M. Elvers, J. Endres, C. Fransen, J. Kotila, O. Möller, A. Richter, T.R. Rodríguez *et al.*, Phys. Rev. Lett. **111**, 172501 (2013)
[15] D. Bohle, A. Richter, W. Steffen, A. Dieperink, N. Lo Iudice, F. Palumbo, O. Scholten, Phys. Lett. B **137**, 27 (1984)
[16] K. Heyde, P. von Neumann-Cosel, A. Richter, Rev. Mod. Phys. **82**, 2365 (2010)
[17] F. Iachello, A. Arima, *The Interacting Boson Model* (Cambridge University Press, Cambridge, 1987)
[18] J. Hammer, B. Fischer, H. Hollick, H. Trautvetter, K. Kettner, C. Rolfs, M. Wiescher, Nucl. Instrum. Methods **161**, 189 (1979)
[19] V. Werner, *Suche nach gemischtsymmetrischen Zuständen in den Kernen ^{96}Mo und ^{82}Se und Untersuchung der Deformation schwerer Kerne* (Diplomarbeit, Institut für Kernphysik, Universität zu Köln, 2002)
[20] H.R. Weller, M.W. Ahmed, H. Gao, W. Tornow, Y.K. Wu, M. Gai, R. Miskimen, Prog. Part. Nucl. Phys. **62**, 257 (2009)
[21] N. Pietralla, Z. Berant, V.N. Litvinenko, S. Hartman, F.F. Mikhailov, I.V. Pinayev, G. Swift, M.W. Ahmed, J.H. Kelley, S.O. Nelson *et al.*, Phys. Rev. Lett. **88**, 012502 (2001)
[22] B. Löher, V. Derya, T. Aumann, J. Beller, N. Cooper, M. Duchene, J. Endres, E. Fiori, J. Isaak, J. Kelley *et al.*, Nucl. Instrum. Meth. A **723**, 136 (2013)
[23] T. Beck, J. Beller, N. Pietralla, M. Bhike, J. Birkhan, V. Derya, U. Gayer, A. Hennig, J. Isaak, B. Löher *et al.*, Phys. Rev. Lett. **118**, 212502 (2017)
[24] N. Pietralla, P. von Brentano, R.D. Herzberg, U. Kneissl, N. Lo Iudice, H. Maser, H.H. Pitz, A. Zilges, Phys. Rev. C **58**, 184 (1998)
[25] H. Pai, T. Beck, J. Beller, R. Beyer, M. Bhike, V. Derya, U. Gayer, J. Isaak, Krishichayan, J. Kvasil *et al.*, Phys. Rev. C **93**, 014318 (2016)
[26] K. Krane, R. Steffen, R. Wheeler, Atom. Data Nucl. Data **11**, 351 (1973)
[27] S. Agostinelli, J. Allison, K. Amako, J. Apostolakis, H. Araujo, P. Arce, M. Asai, D. Axen, S. Banerjee, G. Barrand *et al.*, Nucl. Instrum. Meth. A **506**, 250 (2003)
[28] J. Allison, K. Amako, J. Apostolakis, H. Araujo, P.A. Dubois, M. Asai, G. Barrand, R. Capra, S. Chauvie, R. Chytracek *et al.*, IEEE T. Nucl. Sci. **53**, 270 (2006)
[29] J. Allison, K. Amako, J. Apostolakis, P. Arce, M. Asai, T. Aso, E. Bagli, A. Bagulya, S. Banerjee, G. Barrand *et al.*, Nucl. Instrum. Meth. A **835**, 186 (2016)
[30] J. Chen, J. Cameron, B. Singh, Nucl. Data Sheets **112**, 2715 (2011)
[31] J. Cameron, J. Chen, B. Singh, N. Nica, Nucl. Data Sheets **113**, 365 (2012)
[32] H. Junde, H. Su, Y. Dong, Nucl. Data Sheets **112**, 1513 (2011)
[33] B.A. Brown, W.D.M. Rae, Nucl. Data Sheets **120**, 115 (2014)
[34] M. Honma, T. Otsuka, T. Mizusaki, M. Hjorth-Jensen, Phys. Rev. C **80**, 064323 (2009)